Controllable Generation of Nitric Oxide by Near-Infrared-Sensitized Upconversion Nanoparticles for Tumor Therapy

Xiao Zhang, Gan Tian, Wenyan Yin, Liming Wang, Xiaopeng Zheng, Liang Yan, Jinxia Li, Haoran Su, Chunying Chen, Zhanjun Gu,* and Yuliang Zhao**

$NaYbF_4$:Tm@$NaYF_4$:Yb/Er upconversion nanoparticles are synthesized and then integrated with light-sensitive nitric oxide (NO) donors (Roussin's black salt) to construct a novel near-infrared (NIR)-triggered on-demand NO delivery platform. This nanocompound can absorb 980 nm NIR photons, convert them into higher energy photons and then transfer the energy to the NO donors, resulting in an efficient release of NO. By manipulating the output power of the 980-nm NIR light, NO-concentration-dependent biological effects for cancer therapy can be fine-tuned, which is investigated and confirmed in vitro. High concentrations of NO can directly kill cancer cells and low concentrations of NO can act as a potent P-glycoprotein (P-gp) modulator to overcome multi-drug resistance (MDR) if combined with chemotherapy.

1. Introduction

Light-controlled generation of cytotoxic species for therapeutic applications has attracted a great deal of interest because of its non-invasive nature and high spatiotemporal resolution.[1] The use of light as a trigger can overcome the lack of accuracy of location and sensitivity of a cytotoxic agent, as well as control over the dose and site through modulation of irradiation power and duration.[2] The most successful example of this approach is the use of singlet oxygen ($^1O_2$), a typical cytotoxic agent generated in photodynamic therapy (PDT), which has attracted considerable attention because of its efficiency in damaging proteins and nucleic acid in cells.[3] The process of $^1O_2$ generation requires an optimum incorporation of three key components: the photosensitizer, light, and tissue oxygen.[4] In the case of cancer therapy, the tumor microenvironments are mostly hypoxic, which leads to low productivity of $^1O_2$ and hence limited therapeutic efficacy.[5] Therefore, one of the great challenges in the field is to explore novel photochemical systems that can efficiently generate cytotoxic species at the hypoxic microenvironment of a cancer.

Nitric oxide (NO) is an endogenous gaseous biological mediator that plays a pivotal role in physiological and pathological processes and is also one of the structurally smallest pharmaceutical molecules bearing great potential as an anti-restenosis, wound healing, antibacterial, and anticancer agent.[6] At low concentrations, it acts as a vasodilator in cardiovascular systems, but with increasing concentration it turns into a "killer" that damages mitochondria and DNA by oxidation or nitrosation.[7] By exploiting the flexibility of light stimuli, highly dose-dependent biological effects could be realized and fine-tuned with a light-controlled NO-releasing system.[8] Moreover, photo-generation of NO relies on a photochemical reaction with consequent degradation of the photoactive center, which is independent of influences from the surroundings. Another advantage of a photo-controlled NO delivery system is the low side-effects because NO is only produced and consumed in irradiated tissue. Due to its transitory half-life (ca. 5 s) and short diffusion radius (40–200 μm), it will hardly affect nearby healthy tissue.[9] So far, a number of pioneer studies have focused on photo-controlled NO delivery with multifarious NO-donors. For example, Sortino, Ford, and other researchers fabricated a variety of photo-controlled NO-delivering molecular assemblies, including nanostructured films, polymers, and nanoparticles, and these assemblies exhibit excellent performance in NO-releasing therapeutic applications.[10] Such systems are successful in many applications, and the most efficient photo-released NO donors commonly require direct excitation by UV/blue light. However, the tissue penetration depth of UV/blue light restricts their application to efficient therapy of solid tumors in vivo. Therefore, the main challenge for making photo-released NO treatment clinically applicable for cancer therapy remains tuning the excitation wavelength so that it falls into the "therapeutic window" (650–1100 nm), which is a suitable range for deep tissue treatment.[11] Recently,

Dr. X. Zhang, Dr. G. Tian, Prof. W. Yin, Prof. L. Wang, Dr. X. Zheng, Dr. L. Yan, Dr. J. Li, Prof. H. Su, Prof. C. Chen, Prof. Z. Gu, Prof. Y. Zhao
Key Laboratory for Biomedical Effects of Nanomaterials and Nanosafety
Institute of High Energy Physics and National Center for Nanosciences and Technology
Chinese Academy of Sciences
Beijing, P.R. China
E-mail: tiangan@ihep.ac.cn; zjgu@ihep.ac.cn; yuliangzhao@ihep.ac.cn

Dr. G. Tian
College of Chemistry
Sichuan University
Chengdu 610064, P. R. China
E-mail: tiangan@ihep.ac.cn

Dr. X. Zheng
College of Materials Science and Opto-electronic Technology
University of Chinese Academy of Sciences
Beijing 100049, P. R. China

DOI: 10.1002/adfm.201404402

lanthanide ion (Ln^{3+}) doped upconversion nanoparticles (UCNPs) were found to efficiently harvest incident near-infrared (NIR) photons and upconvert them into higher energy UV–vis photons, which demonstrated that NO precursors can be sensitized in the "therapeutic window".[12] In that system, the UCNPs could serve as a transducer to activate light-sensitive NO precursors through the energy transfer (ET) process under NIR stimuli.[13]

In this work, we chemically synthesized and developed the mesoporous-silica-coated white-light emitting UCNPs ($NaYbF_4$:Tm@$NaYF_4$:Yb/Er) as the NIR photosensitizing platform for dose-controllable NO release by using photolytic $[NH_4][Fe_4S_3(NO)_7]$ (Roussin's black salt, RBS) as the NO-donors (**Scheme 1**). The mesoporous shell could efficiently adsorb the RBS onto UCNPs, while the white upconverted emission results in a maximum spectrum overlap with the RBS absorbance, and then induces efficient photolysis to produce NO under 980-nm laser irradiation via an ET process. Furthermore, we realized an on-demand release of NO by simply regulating the output of the laser power. It is known that the different levels of NO in physiological processes have different physiological functions. In the present work, we have demonstrated that the high concentration of NO produced by higher NIR power irradiation can directly kill cancer cells, whereas a low concentration of NO does not have the potent cell-killing ability but it can significantly inhibit the P-glycoprotein (P-gp) expression on the membrane in multi-drug resistant cancer cells and may thus overcome the multidrug resistance in chemotherapy.

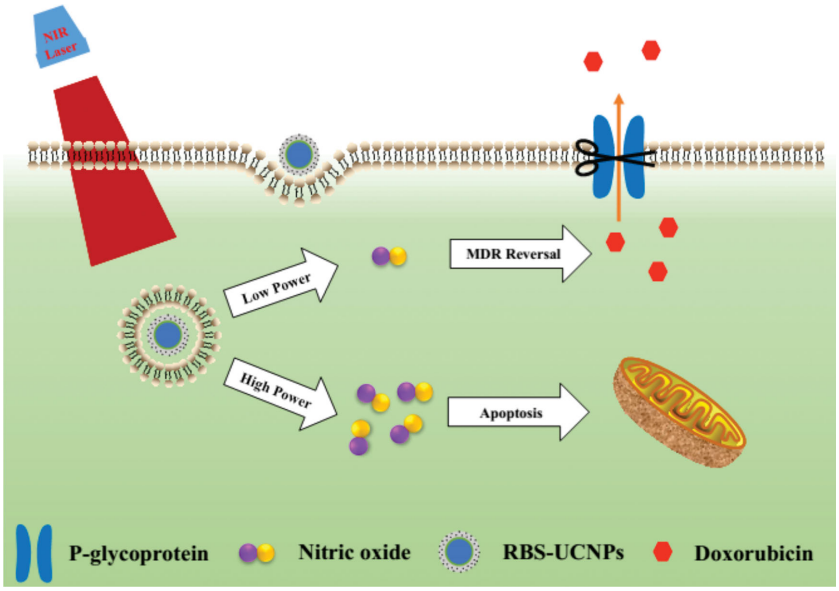

Scheme 1. Schematic illustration of 980-nm NIR light-triggered on-demand NO release for dose-dependent therapeutic applications.

2. Results and Discussions

2.1. Characterization of UCNPs

Figure 1a shows the synthesis routeof RBS-loaded UCNPs and the NIR-triggered release of NO from the nanoplatforms. For the efficient activation of the NO precursor (RBS), hexagonal-phase core–shell structured $NaYbF_4$:Tm@$NaYF_4$:Yb/Er UCNPs with strong white upconversion emission were synthesized via the thermal decomposition method published in one of our previous studies.[14] Figure 1b shows that the monodisperse core-only $NaYbF_4$:Tm UCNPs are spherical and have an average diameter of about 40 nm. After being coated with a layer of $NaYF_4$:Yb/Er, the core/shell structure can be distinguished clearly in the TEM image because of the different electron penetrability between the cores and the shells; the diameter of the final nanoparticles increases to about 70 nm (Figure 1c). The XRD patterns indicate that the as-prepared UCNPs can be well indexed to the hexagonal $NaYbF_4$ (JCPDS No. 27–1427) and no impurities are detected (Figure S1 in the Supporting Information).[15] The growth of a $NaYF_4$:Yb/Er shell not only significantly enhances the UCL intensity (about 12 times higher than that of the core only), but also provides additional emission peaks that preferably match the absorption spectra of RBS (Figure 1g) for efficient ET from UCNPs to RBS, thereby enhancing the RBS photolysis efficacy for NO production. In order to make these hydrophobic NPs water-soluble and capable of RBS loading, a mesoporous silica layer of about 10 nm thickness was decorated on the surface of the as-prepared UCNPs (Figure 1d,e). The mesoporosity could be further confirmed by the N_2 adsorption–desorption measurement. As shown in Figure 1f, the sample exhibits a typical type-IV isotherm with hysteresis at low pressure (0.4–0.6), indicating a mesoporous character.[16] Moreover, the pore-size distribution shows a narrow apex centered at 2.8 nm (Figure 1f inset). These results show that the as-prepared mesoporous-silica-coated UCNPs ($m$$SiO_2$-UCNPs) have mesoporous channels for RBS loading. Drug loading was performed by soaking $m$$SiO_2$-UCNPs with RBS solutions under overnight stirring. The saturated loading capacity (w/w%) calculated from the UV–vis absorption spectra was found to be 10% (Figure S2 of the Supporting Information). The color of the resulting RBS-loaded UCNPs (RBS-UCNPs) complex was brown, and after centrifugation nearly faded supernatant and brown precipitate was observed, indicating the successful loading of RBS onto $m$$SiO_2$-UCNPs (Figure 1h inset). Figure 1h shows the spectral changes of the UCNPs before and after RBS loading, a remarkable fluorescence quenching was observed, in particular for the two emission peaks at 365 and 450 nm, revealing the occurrence of energy transfer from the UCNPs (donors) to RBS (acceptors). In addition, the RBS-UCNPs complex could be well stored in physiological solution with no apparent RBS leakage (Figure S3 in the Supporting Information), making them quite suitable for biological applications.

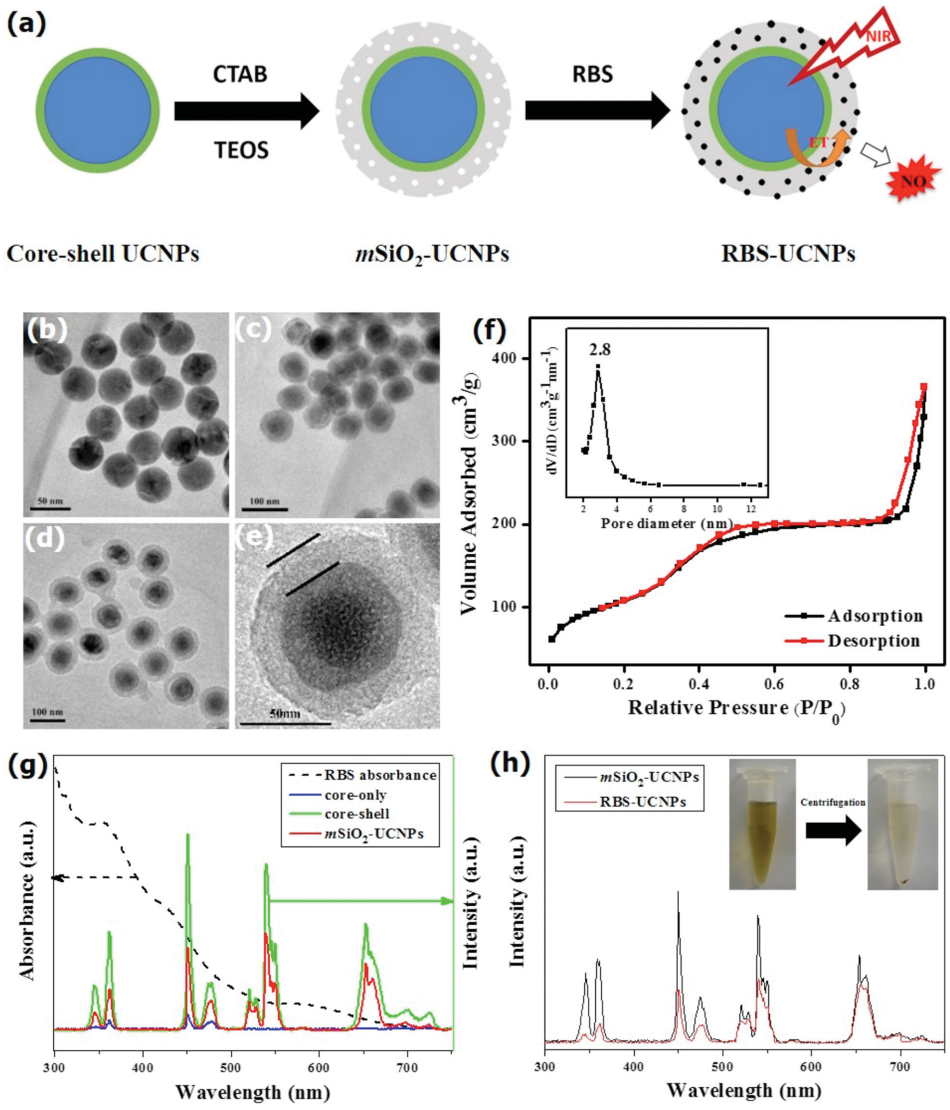

Figure 1. Synthesis and characterization of RBS-UCNPs nanoparticles. a) Schematic illustration of the synthesis of the RBS-UCNPs nanocompound. TEM images of b) core $NaYbF_4$:Tm, c) core/shell structure $NaYbF_4$:Tm@$NaYF_4$:Yb/Er, d) $m$$SiO_2$-UCNPs, and e) a single mSiO_2 UCNP. f) Nitrogen adsorption–desorption isotherms and Barrette–Joynere–Halenda (BJH) pore size distribution curves (inset) of $m$$SiO_2$-UCNPs. g) Fluorescence spectra of core-only UCNPs (blue), core/shell UCNPs (green) and $m$$SiO_2$-UCNPs (red), and UV–vis absorption of RBS (dashed line). h) Fluorescence spectra of UCNPs before (black) and after (red) loading RBS. Inset: photographs of RBS-UCNPs aqueous dispersion before (left) and after (right) centrifugation.

2.2. The On-Demand NO Release from the Nanosystem

We evaluated the RBS-UCNPs complex's "on demand" photo-release behavior of NO upon 980 nm NIR irradiation. Quantitative detection of the NO release from the nanocomplex was carried out by an accurate electrochemistry analysis using a NO-sensitive electrode. The as-prepared RBS-UCNPs were re-dispersed in PBS solution (50 μg mL^{-1}) and irradiated with a 980 nm CW laser at ambient temperature under continuous stirring. Immediate bursts of NO release upon irradiation for short intervals and the "on/off" feature of the NIR-triggered NO generation was clearly evidenced (**Figure 2**a), indicating a fast and agile response to the NIR trigger. In addition, the amount of NO generated from the RBS-UCNPs accumulated with the increase in irradiation time and laser output power, as shown in Figure 2b. These results clearly showed that the dose-controllable release of NO could be realized by manipulating the NIR laser output, favoring a dose-dependent biological application. One critical aspect of NO delivery systems is their permeability through cell membranes, which can significantly enhance the cellular uptake at interested sites. Intracellular fluorescence imaging of in situ NO generation in HeLa cells was performed using a commercial NO indicator, 3-amino-4-aminomethyl-2′, 7′-difluorescein, diacetate (DAF-FM). As shown in Figure 2c, blue fluorescence represents a cell nucleus labeled with Hoechst 33342 whereas green fluorescence that originates from DAF-FM indicates the generation of NO in cells. Only when treated with both RBS-UCNPs and 980-nm laser irradiation,

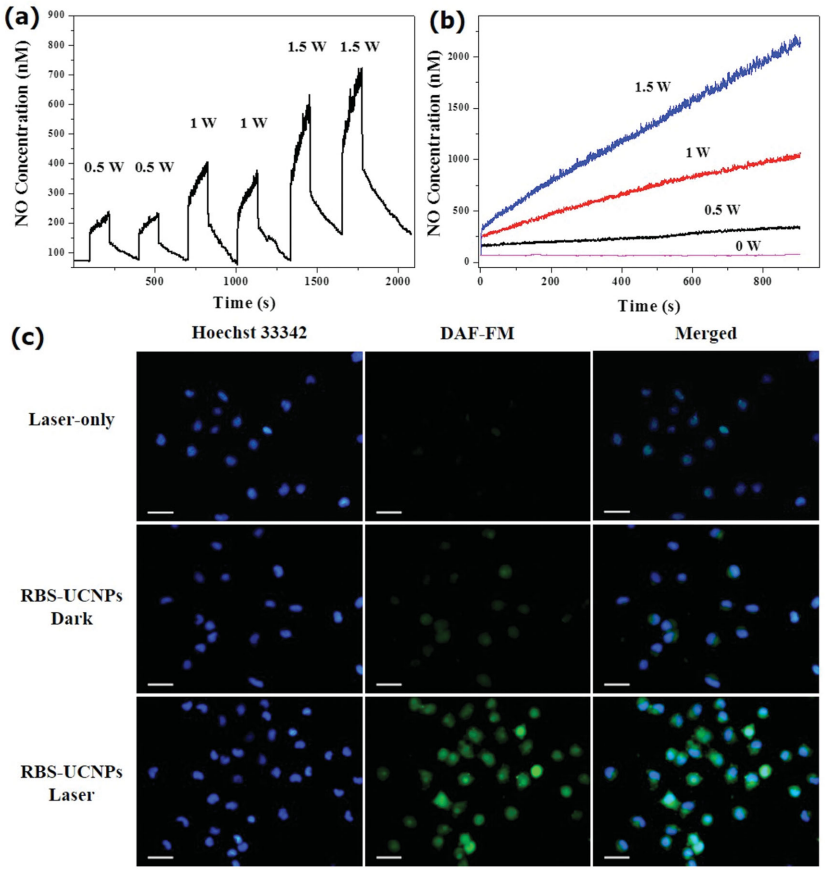

Figure 2. Detection of the NO release. a) On/off behavior of the NO generation induced by 980 nm laser irradiation for different power outputs. b) Generation of NO as a function of the irradiation time for different power outputs. c) Fluorescent images of Hela cells stained with Hoechst 33342 and DAF-FM (a NO fluorescent probe) upon being treated with RBS-UCNPs under dark conditions or 980 nm irradiation (1 W cm^{-2}, 5 min). The scale bar is 50 μm.

a sufficient amount of NO was generated, proving that RBS-UCNPs can enter into the cells and release NO in situ under 980 nm laser irradiation.

2.3. Estimation of the NO Sensitized PDT Effect

The controllable and steady NO generation encouraged us to investigate their dose-dependent biological effect. In a proof-of-concept experiment, three different power densities of the 980 nm laser were used. As shown in Figure S4 in the Supporting Information, laser-power regulating cell killing ability was observed for both kinds of tested cancer cells, HeLa and MCF-7. We then systematically evaluated the high-dose NO-induced PDT efficacy in cancer cells treatment. In vitro cytotoxicity estimation against HeLa and MCF-7 was carried out using a CCK-8 assay. As shown in **Figure 3**a and b, *m*SiO_2-UCNPs with or without 980 nm laser irradiation (1 W cm^{-2}, 5 min) exhibited negligible cytotoxicity. When incubated with RBS-UCNPs without 980 nm irradiation, the cell viability of the two types of cells still remained above 80%, which indicated its low dark toxicity. However, under 980 nm irradiation, the cell viability distinctly decreased with the increase of the RBS-UCNPs concentration. The results demonstrated that the NO-based PDT effect of the RBS-UCNPs could be induced by NIR irradiation, and high-dose NO could efficiently kill cancer cells. To intuitively display the killing capacity, live-dead cell staining was performed and the results are shown in Figure 3c. Two different fluorescence dyes represented cells with different status – green representing the live cells and red indicating the dead ones. The experiments with Hela and MCF-7 cells practically gave the same results: using either RBS-UCNPs or the 980 nm laser alone has no significant influence on the cells, whereas the combination of RBS-UCNPs and 980 nm irradiation has a remarkable impact and leads to a large number of dead cells. These observations demonstrated that the cause of cell death could solely be ascribed to the NO-based PDT effect of RBS-UCNPs under 980 nm laser irradiation, which corresponded with our cell viability results.

2.4. Low-Dose NO Induced MRD Reversal

Although a low dose of NO only has weak cancer-cell killing ability (Figure S4 in the Supporting Information), we found that low NO doses can improve the sensitivity of resistant tumor cells towards anticancer drugs when combined with chemotherapy, and thus overcome multi-drug resistance (MDR) to achieve successful cancer treatment. MDR is usually caused by a family of membrane proteins called P-glycoprotein (P-gp), which efflux chemotherapeutic agents out of the tumor cells, thereby decreasing intracellular drug concentrations and pharmacological efficacy.[17] In order to prove that the NO released from RBS-UCNPs could serve as an efficient P-gp inhibitor, we first assessed the uptake amount of doxorubicin (DOX) in MCF-7/DOX^R cells by flow cytometry. As can be seen in **Figure 4**a, the intracellular DOX accumulation increased remarkably after being treated with RBS-UCNPs under 980-nm laser excitation (0.5 W cm^{-2}, 5 min). Next, a western blot was used to detect the expression of the relative proteins in MCF-7/DOX^R cells. After exposure to NO, the expression of P-gp proteins was obviously repressed (Figure 4b). The decreased expression of P-gp will prevent the efflux of drugs, which results in a higher doxorubicin concentration in the cells. Correspondingly, fluorescent images in Figure 4c and d clearly show that the DOX signals from the NO-exposed group was much stronger due to DOX accumulation. Next, we evaluated whether the combination of RBS-UCNPs and DOX (10 μM) could effectively overcome MDR and achieve successful antitumor effects in MCF-7/DOX^R cells. From Figure 4e it is clear that the MCF-7/DOX^R cells had a strong drug resistance in view of the above-95% survival at a DOX dosage of 10 μM. In addition, the RBS-UCNPs also showed

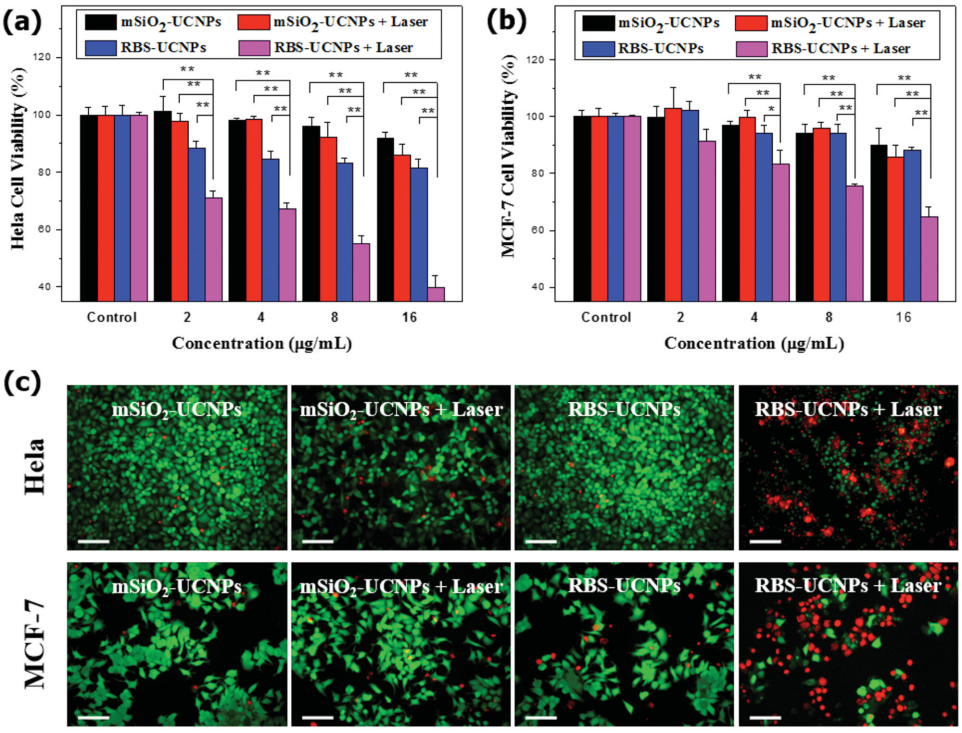

Figure 3. Estimation of the NO-sensitized PDT effect. In vitro cytotoxicity analysis of $mSiO_2$-UCNPs, RBS-UCNPs in the dark or under 980 nm irradiation for 5 min on a) Hela cells and b) MCF-7 cells. Error bars were based on triplicated samples. $*P < 2\ 0.05$, $**\ P < 0.01$. c) Fluorescent images of Hela and MCF-7 cells with live-dead staining after different treatments. The power density and irradiation time are 1 W cm^{-2} and 5 min, respectively. The scale bar is 100 μm.

no obvious cytotoxic effect under 980 nm irradiation due to the decrease of the NO dose by reducing the laser output power density (0.5 W cm^{-2}). While the cell viability decreased sharply when the cells were simultaneously treated with DOX and RBS-UCNPs under 980-nm irradiation, a synergistic effect occurred in the case of the combined delivery of NO and DOX for MDR reversal.

3. Conclusion

In summary, we have successfully synthesized white-emitting $NaYbF_4$:Tm@$NaYF_4$:Yb/Er UCNPs as transducers and developed a new NIR-triggered NO release platform based on photolysis by way of RBS. The results demonstrated that $NaYbF_4$:Tm@$NaYF_4$:Yb/Er UCNPs provide an ideal platform that (i) could efficiently sensitize NO release in a "therapeutic window" required for deep tumor therapy, and (ii) could realize an on-demand and dose-controllable NO-release. By regulating the output of the laser power, we also evaluated the dose-dependent pharmacological effects of NO for cancer therapy. Potent inhibition of tumor cell growth was revealed under higher power irradiation. On the other hand, a low dose of NO generated under lower power irradiation is demonstrated to serve as an efficient P-gp inhibitor for multi-drug resistance reversal when combined with chemotherapy. Thus, the present work may bring opportunities for the development of a NO-based cancer therapy, and provides new insights for further exploration on a synergetic strategy that combines the controlled release of therapeutic amounts of NO with other existing cancer therapeutics.

4. Experimental Section

Materials: Lanthanide (Ln) oxides (Ln_2O_3, 99.9%, Ln: Y, Yb, Er), Ln nitrate hydrates ($Ln(NO_3)_3$, 99.9%, Ln: Yb, Tm), trifluoroacetic acid (TFA), sodium trifluoroacetate (98%), oleic acid (OA, 90%), 1-octadecene (ODE, 90%), ammonium fluoride (NH_4F, 96%), sodium hydroxide (NaOH, 98%), tetraethoxysilane (TEOS, 98%), sodium nitrite ($NaNO_2$, 97%), iron(II) sulfate heptahydrate ($FeSO_4{\cdot}7H_2O$, 98%) and ammonium hydroxide (NH_4OH, 28% NH_3) were purchased from Alfa Aesar Ltd. Sodium oleate (98%) was provided by Aladdin Inc. Cetyltrimethyl ammonium bromide (CTAB, 99%) was purchased from Sinopharm Chemical Reagent Co., Ltd. Cyclohexane and ethanol were supplied from the Beijing Chemical Reagent Company. Hoechst 33342 and 3-Amino,4-aminomethyl-2′,7′-difluorescein, diacetate (DAF-FM DA) were bought from the Beyotime Institute of Biotechnology. Cell counting kit-8 (CCK-8), Calcein-AM (CA) and propidium iodide (PI) were provided by Dojindo Laboratories in Japan. All chemicals were analytical grade and used without further purification. Deionized water was used in all experiments.

Preparation of the Lanthanide-Oleate Precursor: The lanthanide-oleate complexes were pre-synthesized by reacting lanthanide nitrate with sodium oleate. In a typical experiment, 20 mmol of ytterbium nitrate and 60 mmol of sodium oleate were dissolved in a mixture of ethanol (40 mL), distilled water (40 mL), and cyclohexane (80 mL). After stirring for 24 h at room temperature, the mixture was statically separated. The upper organic layer including the ytterbium-oleate complex was collected and washed three times with a water: ethanol (1:1) solution. The remaining water, ethanol, and cyclohexane in the organic layer were evaporated under reduced pressure, yielding the ytterbium-oleate

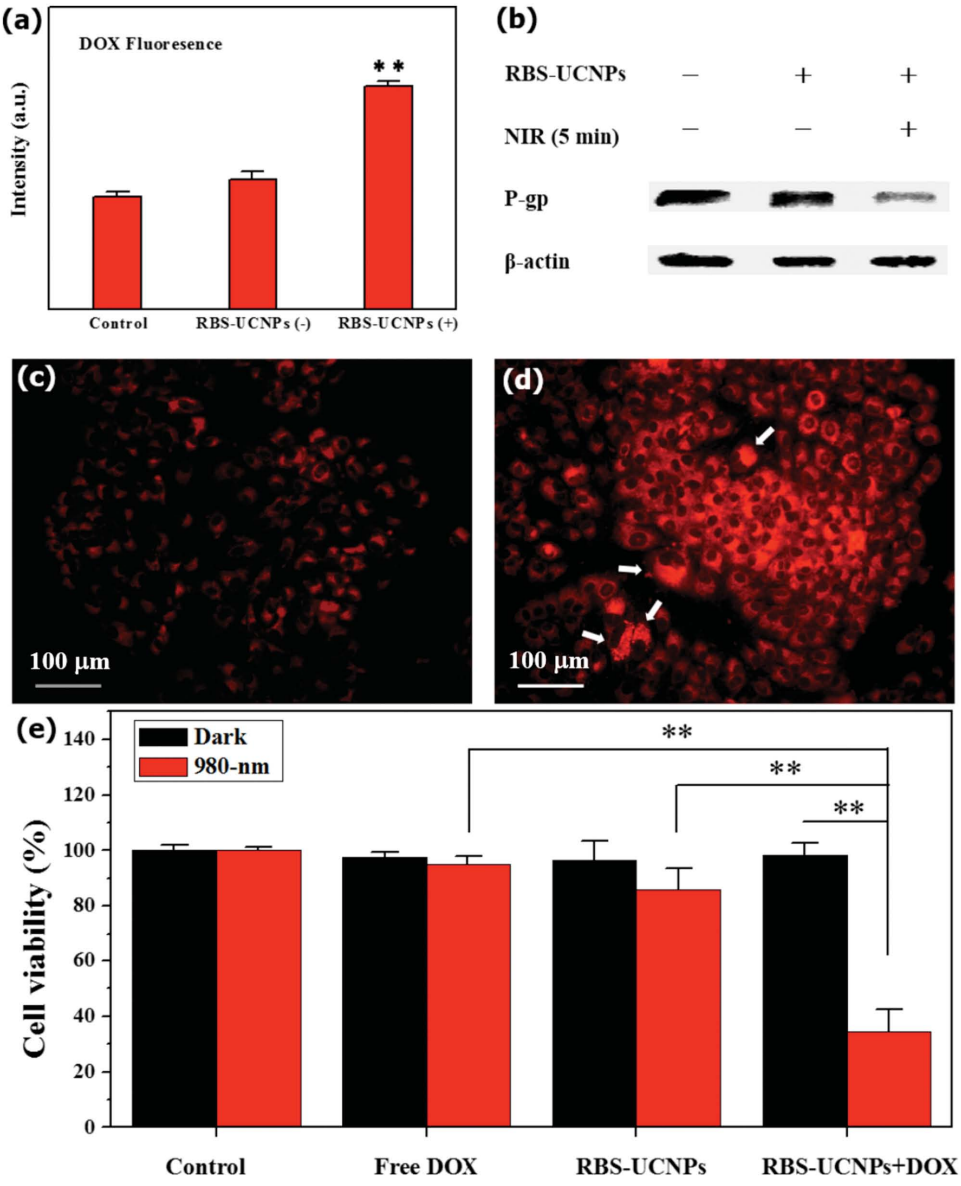

Figure 4. NO-induced MDR reversal. a) Effect of the NO on P-gp inhibition determined by the flow-cytometric assessment of the DOX uptake in MCF-7-DOX^R cells. b) Western blot for the detection of P-gp expression. Fluorescent images of c) the MCF-7/DOX^R cells treated with free DOX and d) the mixture of DOX and RBS-UCNPs under 980-nm irradiation. e) Cytotoxicity assay in MCF-7/DOX^R under different treatments. Error bars were based on triplicated samples. $^{**}P < 0.01$. 980 nm power density: 0.5 W cm^{-2}, time: 5 min.

complex in a waxy solid form. The complex was finally re-dissolved in a quantitative OA and ODE for later use.

Preparation of Lanthanide Trifluoroacetate Precursor: In a typical synthesis of the yttrium trifluoroacetate, 10 mmol of Y_2O_3 was added to a mixture of 50 mL of distilled water and 50 mL of TFA. The mixture was stirred at 85 °C until the solution was clear. The final product was obtained after evaporating the redundant TFA and water at 70 °C and stored in a desiccator.

Synthesis of Core NaYbF$_4$:Tm UCNPs: NaYbF$_4$:Tm nanoparticles (UCNPs) were synthesized following the methods reported by Liu et al.[18] 0.995 mmol of Yb-oleate, 0.005 mmol of Tm-oleate, 2.5 mmol of NaOH and 4 mmol of NH_4F were added into a mixed solution of OA (6 mL) and ODE (15 mL) in a 50 mL single-necked flask. The mixture was heated to 110 °C and vacuumed for 40 min to remove water and oxygen. Then the reaction was rapidly heated to 305 °C under an argon atmosphere for 60 min with stirring. After cooling to room temperature, the product was collected by centrifugation and washed three times with ethanol. Finally, the obtained UCNPs were dispersed in cyclohexane for further use.

Synthesis of Core/Shell NaYbF$_4$:Tm@NaYF$_4$:Yb/Er UCNPs: 0.4 mmol of core UCNPs dispersed in 3 mL of OA were added into a mixture of $Y(CF_3COO)_3$ (0.3 mmol), $Yb(CF_3COO)_3$ (0.1 mmol), $Er(CF_3COO)_3$ (0.004 mmol), $NaCF_3COO$ (0.4 mmol), OA (3 mL) and ODE (15 mL). The mixture was kept at 110 °C under vacuum for 40 min to eliminate water, oxygen and cyclohexane. Afterwards, it was heated to 295 °C under an argon atmosphere for 45 min. The final product was isolated by centrifugation and washed with ethanol for three times.

Synthesis of Mesoporous SiO$_2$-coated UCNPs: Mesoporous SiO_2 was chosen to modify the core/shell UCNPs according to a previously reported literature.[19] Typically, 20 mg of core/shell UCNPs dispersed in 4 mL of cyclohexane were added into a mixture of CTAB (0.1 g) and distilled water (15 mL) and then heated to 80 °C with stirring in order to

remove cyclohexane. After the solution is transparent, 10 mL of CTAB-UCNPs were dropped into a mixed solution containing of 20 mL of distilled water, 3 mL of ethanol and 150 µL of NaOH (2 mol mL^{-1}), and then the mixture were heated to 70 °C under stirring. 150 µL of TEOS was added dropwise and the reaction was kept 70 °C for 10 min. The product was obtained after centrifugation at 12 000 rpm for 8 min and purified by washing with ethanol for 3 times. Finally, the CTAB molecules were removed with an iron exchange method. The as-prepared product was added into a mixture of 0.3 g of NH_4NO_3 and 50 mL of ethanol, and the reaction was kept at 60 °C for 2 h. The mesoporous SiO_2-coated UCNPs were collected by centrifugation and washed with water several times.

Synthesis of Roussin's Black Salt: Roussin's Black Salt ($[NH_4][Fe_4S_3(NO)_7]$) was synthesized according to previous work reported by Seyferth et al.[20] 4.5 g of $NaNO_2$ dissolved in 20 mL of distilled water and 5 mL of $(NH_4)_2S$ in 15 mL of distilled water were added into a 250 mL flask. The yellow solution was heated under stirring until the solution turned dark red. 10 g of $FeSO_4$ in 80 mL of distilled water was added to the first solution. And then 12.5 mL of NH_4OH solution was dropped into the flask. The reaction was heated to 90 °C at reflux for 10 min and then filtered. The black-brown solution was kept in 4 °C overnight and the black crystalline solid was collected and freeze-dried.

Characterization: The morphology of the as-synthesized nanoparticles were observed on field emission transmission electron microscopes (TEM, Tecnai G2 20 St). X-ray diffraction (XRD) patterns of the nanoparticles were characterized by a Japan Rigaku D/max-2500 diffractometer with Cukα radiation (λ = 1.5418Å). Nitrogen adsorption-desorption isotherms were obtained by a Micromeritics ASAP2020 (Micromeritics Instrument LTD.) at 108 K. The Brunauer–Emmett–Teller (BET) method was utilized to calculate the specific surface area by using adsorption data in the range of the relative pressures from 0.01 to 1.00. The pore-size distributions were calculated using the Barrett–Joyner–Halanda (BJH) method. The photoluminescence spectra were measured by a fluorescence spectrophotometer (Horiba Jobin Yvon FluorolLog3). The UV–vVis absorption data was collected by U-3900 spectrophotometer (HITACHI).

Drug Loading and Stability Study: RBS was loaded in the mesoporous silica shell of UCNPs by an impregnation method. In a typical experiment, 10 mg of *m*SiO_2-UCNPs was dispersed in 20 mL of distilled water that contained different concentrations of RBS in brown vials. After stirring for 24 h in dark conditions, the brown product was collected by centrifugation and washed for several times. Netx, the UV-vis absorption spectra of the supernatant was measured. The loading amounts were calculated according to the standard curves of RBS at varying concentrations. The stability of RBS-UCNPs was studied by measuring the released amount of RBS. 5 mg of RBS-UCNPs was re-dispersed in distilled water (10 mL) and shaken at 37 °C under dark conditions. At certain time intervals, 3 mL of the medium was taken out to determine the UV-vis spectra and then returned to the original medium. The released amount of RBS was calculated from the changes in absorbance.

Nitric Oxide Detection: Nitric oxide was detected and quantified using a Free Radical Analyzer (TBR 1025) with a NO-sensitized electrode purchased from World Precision Instruments. Before measurement, the standard curve should be established by chemical generation of NO by using 0.1 M H_2SO_4, 0.1 M KI, and 50 µM KNO_2. Next, the as-prepared RBS-UCNPs were dispersed in PBS solution (50 µg mL^{-1}) and irradiated with a 980 nm CW laser at ambient temperature under continuous stirring. The amount of NO could be calculated by the recorded current.

Intracellular Nitric Oxide Staining: Nitric oxide in cells was stained by a commercial NO indicator, 3-amino-4-aminomethyl-2′,7′-difluorescein, diacetate (DAF-FM). Hela cells were seeded in 6-well plates at 40 000 cells per well. After the cells were adherent, the cells were treated with the DAF-FM solution (5 µM, 1 mL) at 37 °C for 30 min. And then the cells were treated with RBS-UCNPs for 2 h and irradiated for 5 min. The stained cells were analyzed using inverted fluorescence microscopy (IX73, Olympus, Japan).

In Vitro Cytotoxicity Study of mSiO_2-UCNPs: The viability of Hela and MCF-7 was assessed by a CCK-8 assay. The cells were cultured in IMDM medium with 10% FBS at 37 °C with 5% CO_2. The cells were incubated in 96-well plates at a density of 5000 cells per well. After the cells were adherent, fresh medium containing *m*SiO_2-UCNPs was added and incubated for 24 h. Next, the wells were washed with PBS buffer twice and incubated with fresh medium containing CCK-8 for another 2 h. The absorbance was determined with a Thermo Multiskan MK3 reader at 450 nm. Three independent experiments were performed, and for each concentration experiments were carried out in sixfold.

NO Based PDT Effect of RBS-UCNPs: The NO-based PDT effect of RBS-UCNPs was assessed by CCK-8 assays. Hela and MCF-7 cells were incubated in 96-well plates with a density of 5000 cells per well. After the cells were adherent, different concentrations of RBS-UCNPs were added and incubated for 2 h. The original medium was then replaced with fresh medium, and subsequently irradiated with a 980 nm laser with different power densities for 5 min. After 12 h, the wells were washed with PBS buffer and incubated with CCK-8 for 2 h. The absorbance was determined with a Thermo Multiskan MK3 reader at 450 nm. Three independent experiments were performed and for each concentration experiments were performed in sixfold. Furthermore, inverted fluorescence microscopy (IX73, Olympus, Japan) was used to visualize cells stained with live-dead stains (Calcein-AM and PI).

Synergy Effect of NO-based PDT and DOX: MCF-7/DOX^R cells were adopted for studying the synergy effect of NO-based PDT and chemotherapy. The cells were seeded in 96-well plates at 5000 cells per well. Then, the cells were treated with different concentrations of RBS-UCNPs for 2 h and irradiated with a 980 nm laser for 5 min after replacing the original medium. The cells were exposed to doxorubicin (10 µM, 1 mL) for 12 h, and next fresh medium that contained CCK-8 was added for 2 h. The absorbance was measured with a Thermo Multiskan MK3 reader at 450 nm. At least three independent experiments were performed and for each concentration experiments were performed in sixfold.

Intracellular Doxorubicin Accumulation Assay: Flow cytometry was used to detect the intracellular doxorubicin accumulation in MCF-7/DOX^R cells. The cells were seeded into 6-well plates at 50000 cells per well. The cells were treated with RBS-UCNPs (10 µg mL^{-1}, 1 mL) for 2 h. After irradiation with a 980 nm laser (0.5 W cm^{-2}) for 5 min, the cells were exposed to doxorubicin (10 µM, 1 mL) for another 2 h. Subsequently, the cells were washed three times with 4 °C PBS buffer, and then digested and collected. The data were acquired by flow cytometry (Accuri c6, BD, USA).

Western Blot Assay: The effect of RBS-UCNPs on inhibiting P-gp expression in MCF-7/DOX^R cells was measured by Western blot assay. MCF-7/MDR cells were incubated in 6-well plates with a density of 50 000 per well. After being treated with RBS-UCNPs for 4 h and irradiated for 5 min, the cells were lysed and harvested after centrifugation. The cell lysates (25 µg per lane) were separated by SDS-PAGE (10% gel) and transferred onto nitrocellulose membranes (PVDF). The PVDF membranes were incubated in 5% skimmed milk solution at 37 °C for 1 h, and then incubated with relevant primary antibodies (diluted 1:2000) for P-gp and β-actin at 4 °C overnight. After washing, the PVDF membranes were incubated with HRP-labeled secondary antibodies (diluted 1:10 000) at 37 °C for 1 h. Finally, the membranes were stained by an ECL detection kit and then photographed using the FluorChem HD2 Chemilumilescent Imaging System (ProteinSimple, USA).

Supporting Information

Supporting Information is available from the Wiley Online Library or from the author.

Acknowledgements

This work was supported by the 973 program (2012CB932504 and 2015CB932104), and NSFC (21001108, 21101158, and 21320102003).

Received: December 12, 2014
Revised: March 12, 2015
Published online: April 11, 2015

[1] a) T. Liu, C. Wang, X. Gu, H. Gong, L. Cheng, X. Shi, L. Feng, B. Sun, Z. Liu, *Adv. Mater.* **2014**, *26*, 3433; b) Z. Zhang, J. Wang, C. Chen, *Adv. Mater.* **2013**, *25*, 3869; c) X. Yue, C. O. Yanez, S. Yao, K. D. Belfield, *J. Am. Chem. Soc.* **2013**, *135*, 2112; d) J. Yang, D. Shen, L. Zhou, W. Li, X. Li, C. Yao, R. Wang, A. M. El-Toni, F. Zhang, D. Zhao, *Chem. Mater.* **2013**, *25*, 3030; e) K. L. Ciesienski, K. J. Franz, *Angew. Chem. Int. Ed.* **2011**, *50*, 814; f) S. Wang, R. Gao, F. Zhou, M. Selke, *J. Mater. Chem.* **2004**, *14*, 487.

[2] a) N. M. Idris, M. K. G. Jayakumar, A. Bansal, Y. Zhang, *Chem. Soc. Rev.* **2014**, *44*, 1449; b) X. Yang, X. Liu, Z. Liu, F. Pu, J. Ren, X. Qu, *Adv. Mater.* **2012**, *24*, 2890; c) C. Wang, L. Cheng, Y. Liu, X. Wang, X. Ma, Z. Deng, Y. Li, Z. Liu, *Adv. Funct. Mater.* **2013**, *23*, 3077; d) W. Fang, J. Yang, J. Gong, N. Zheng, *Adv. Funct. Mater.* **2012**, *22*, 842.

[3] a) G. Tian, W. Ren, L. Yan, S. Jian, Z. Gu, L. Zhou, S. Jin, W. Yin, S. Li, Y. Zhao, *Small* **2013**, *9*, 1929; b) N. M. Idris, M. K. Gnanasammandhan, J. Zhang, P. C. Ho, R. Mahendran, Y. Zhang, *Nat. Med.* **2012**, *18*, 1580; c) L. Pan, J. Liu, J. Shi, *Adv. Funct. Mater.* **2014**, *24*, 7318.

[4] a) V. Rapozzi, E. Della Pietra, S. Zorzet, M. Zacchigna, B. Bonavida, L. E. Xodo, *Nitric Oxide* **2013**, *30*, 26; b) H. I. Pass, *J. Natl. Cancer Inst.* **1993**, *85*, 443.

[5] M. Höckel, P. Vaupel, *J. Natl. Cancer Inst.* **2001**, *93*, 266.

[6] a) D. A. Wink, J. B. Mitchell, *Free Radical Biol. Med.* **1998**, *25*, 434; b) L. J. Ignarro, G. M. Buga, K. S. Wood, R. E. Byrns, G. Chaudhuri, *Proc. Natl. Acad. Sci.* **1987**, *84*, 9265.

[7] a) A. W. Carpenter, M. H. Schoenfisch, *Chem. Soc. Rev.* **2012**, *41*, 3742; b) D. A. Wink, Y. Vodovotz, J. Laval, F. Laval, M. W. Dewhirst, J. B. Mitchell, *Carcinogenesis* **1998**, *19*, 711; c) S. Gupta, N. Ahmad, H. Mukhtar, *Cancer Res.* **1998**, *58*, 1785.

[8] S. Sortino, *Chem. Soc. Rev.* **2010**, *39*, 2903.

[9] S. Sortino, *J. Mater. Chem.* **2012**, *22*, 301.

[10] a) J. Xu, F. Zeng, H. Wu, C. Hu, C. Yu, S. Wu, *Small* **2014**, *10*, 3750; b) V. Kirejev, N. Kandoth, R. Gref, M. B. Ericson, S. Sortino, *J. Mater. Chem. B* **2014**, *2*, 1190; c) P. Sudhesh, K. Tamilarasan, P. Arumugam, S. Berchmans, *ACS Appl. Mater. Interfaces* **2013**, *5*, 8263; d) P. C. Ford, *Nitric Oxide* **2013**, *34*, 56; e) D. A. Riccio, M. H. Schoenfisch, *Chem. Soc. Rev.* **2012**, *41*, 3731; f) A. D. Ostrowski, P. C. Ford, *Dalton Trans.* **2009**, 10660; g) J. Bourassa, W. DeGraff, S. Kudo, D. A. Wink, J. B. Mitchell, P. C. Ford, *J. Am. Chem. Soc.* **1997**, *119*, 2853.

[11] a) Y. Zhong, G. Tian, Z. Gu, Y. Yang, L. Gu, Y. Zhao, Y. Ma, J. Yao, *Adv. Mater.* **2014**, *26*, 2831; b) L. Tan, A. Wan, X. Zhu, H. Li, *Chem. Commun.* **2014**, *50*, 5725.

[12] a) L. Zhao, J. Peng, Q. Huang, C. Li, M. Chen, Y. Sun, Q. Lin, L. Zhu, F. Li, *Adv. Funct. Mater.* **2014**, *24*, 363; b) Z. Gu, L. Yan, G. Tian, S. Li, Z. Chai, Y. Zhao, *Adv. Mater.* **2013**, *25*, 3758; c) W. Feng, C. Han, F. Li, *Adv. Mater.* **2013**, *25*, 5287; d) G. Tian, Z. Gu, X. Liu, L. Zhou, W. Yin, L. Yan, S. Jin, W. Ren, G. Xing, S. Li, Y. Zhao, *J. Phys. Chem. C* **2011**, *115*, 23790; e) F. Wang, X. Liu, *Chem. Soc. Rev.* **2009**, *38*, 976; f) F. Chen, W. Bu, S. Zhang, J. Liu, W. Fan, L. Zhou, W. Peng, J. Shi, *Adv. Funct. Mater.* **2013**, *23*, 298.

[13] a) P. T. Burks, J. V. Garcia, R. GonzalezIrias, J. T. Tillman, M. Niu, A. A. Mikhailovsky, J. Zhang, F. Zhang, P. C. Ford, *J. Am. Chem. Soc.* **2013**, *135*, 18145; b) J. V. Garcia, J. Yang, D. Shen, C. Yao, X. Li, R. Wang, G. D. Stucky, D. Zhao, P. C. Ford, F. Zhang, *Small* **2012**, *8*, 3800.

[14] a) L. Zhou, X. Zheng, Z. Gu, W. Yin, X. Zhang, L. Ruan, Y. Yang, Z. Hu, Y. Zhao, *Biomaterials* **2014**, *35*, 7666; b) G. Tian, W. Yin, J. Jin, X. Zhang, G. Xing, S. Li, Z. Gu, Y. Zhao, *J. Mater. Chem. B* **2014**, *2*, 1379.

[15] a) G. Chen, J. Shen, T. Y. Ohulchanskyy, N. J. Patel, A. Kutikov, Z. Li, J. Song, R. K. Pandey, H. Ågren, P. N. Prasad, G. Han, *ACS Nano* **2012**, *6*, 8280; b) S. Zeng, G. Ren, W. Li, C. Xu, Q. Yang, *J. Phys. Chem. C* **2010**, *114*, 10750; c) X. Liang, X. Wang, J. Zhuang, Q. Peng, Y. Li, *Adv. Funct. Mater.* **2007**, *17*, 2757.

[16] a) W. Li, Q. Yue, Y. Deng, D. Zhao, *Adv. Mater.* **2013**, *25*, 5129; b) H. S. Qian, H. C. Guo, P. C. Ho, R. Mahendran, Y. Zhang, *Small* **2009**, *5*, 2285; c) J. Liu, C. Wang, X. Wang, X. Wang, L. Cheng, Y. Li, Z. Liu, *Adv. Funct. Mater.* **2015**, *25*, 384.

[17] a) X. Tang, X. Gu, H. Ai, G. Wang, H. Peng, Y. Lai, Y. Zhang, *Bioorg. Med. Chem. Lett.* **2012**, *22*, 801; b) N. E. Matthews, M. A. Adams, L. R. Maxwell, T. E. Gofton, C. H. Graham, *J. Natl. Cancer Inst.* **2001**, *93*, 1879; c) L. Wang, X. Lin, J. Wang, Z. Hu, Y. Ji, S. Hou, Y. Zhao, X. Wu, C. Chen, *Adv. Funct. Mater.* **2014**, *24*, 4197; d) G. Tian, X. Zhang, X. Zheng, W. Yin, L. Ruan, X. Liu, L. Zhou, L. Yan, S. Li, Z. Gu, Y. Zhao, *Small* **2014**, *10*, 4160; e) M. M. Gottesman, *Cancer Res.* **1993**, *53*, 747.

[18] X. Liu, X. Zhang, G. Tian, W. Yin, L. Yan, L. Ruan, Z. Yang, D. Xiao, Z. Gu, *Cryst. Eng. Commun.* **2014**, *16*, 5650.

[19] Z. Li, Y. Zhang, S. Jiang, *Adv. Mater.* **2008**, *20*, 4765.

[20] D. Seyferth, M. K. Gallagher, M. Cowie, *Organometallics* **1986**, *5*, 539.